The Astrophysical Journal, 654:125–137, 2007 January 1

THE SURVEY OF NEARBY NUCLEI WITH THE SPACE TELESCOPE IMAGING SPECTROGRAPH: EMISSION-LINE NUCLEI AT *HUBBLE SPACE TELESCOPE* RESOLUTION[1]

Joseph C. Shields,[2] Hans-Walter Rix,[3] Marc Sarzi,[4] Aaron J. Barth,[5] Alexei V. Filippenko,[6] Luis C. Ho,[7] Daniel H. McIntosh,[8] Gregory Rudnick,[9,10] and Wallace L. W. Sargent[11]

Received 2004 August 14; accepted 2006 September 8

ABSTRACT

We present results from a program of optical spectroscopy for 23 nearby galaxies with emission-line nuclei. This investigation takes advantage of the spatial resolution of the *Hubble Space Telescope* to study the structure and energetics of the central ~10–20 pc, and the resulting data have value for quantifying central black hole masses, star formation histories, and nebular properties. This paper provides a description of the experimental design, and new findings from the study of emission lines. The sample targets span a range of nebular spectroscopic class, from H II to Seyfert nuclei. This data set and the resulting measurements are unique in terms of the sample size, the range of nebular class, and the investigation of physical scales extending down to parsecs. The line ratios indicative of nebular ionization show only modest variations over order-of-magnitude differences in radius, and demonstrate in a systematic way that geometrical dilution of the radiation field from a central source cannot be assumed as a primary driver of ionization structure. Comparisons between large- and small-aperture measurements for the H II/LINER transition objects provide a new test that challenges conventional wisdom concerning the composite nature of these systems. We also list a number of other quantitative results that are of interest for understanding galaxy nuclei, including (1) the spatial distribution/degree of concentration of Hα emission as a function of nebular type; (2) the radial variation in electron density as a function of nebular type; and (3) quantitative broad Hα estimates obtained at a second epoch for these low-luminosity nuclei. The resulting measurements provide a new basis for comparing the nuclei of other galaxies with that of the Milky Way. We find that the Galactic center is representative across a wide span of properties as a low-luminosity emission-line nucleus.

Subject headings: galaxies: active — galaxies: nuclei — Galaxy: center — Galaxy: nucleus

1. INTRODUCTION

The physical properties of galaxy nuclei are of larger interest in light of growing indications that evolution in the central few parsecs is linked to the global properties of the surrounding galaxy. This connection is evident, particularly in correlations between the mass of a central black hole and bulge mass (e.g., Kormendy & Richstone 1995; Häring & Rix 2004) or velocity dispersion (Gebhardt et al. 2000; Ferrarese & Merritt 2000). Star formation in the centers of galaxies is also known to take on unusual forms that may be in symbiosis with a central mass concentration or the larger structure of the galaxy (i.e., bulge or bar). A rich phenomenology is seen in the central few parsecs of galaxy nuclei within the Local Group, but our knowledge of nuclei at greater distances is limited by a corresponding reduction in spatial resolution. This problem has particularly afflicted ground-based optical spectroscopic studies, which typically sample nuclei with apertures encompassing hundreds of parsecs or more.

To investigate the structure and constituents of galaxy nuclei on small scales, we therefore undertook the Survey of Nearby Nuclei with STIS (SUNNS), a program of *Hubble Space Telescope* (*HST*) narrow-slit spectroscopy for a sample of nearby galaxies outside the Local Group. The target objects were selected on the basis of nebular emission in their centers, and are thus "active" in some sense, although at low levels that are very common in bright galaxies. The SUNNS data are appropriate for addressing several major questions, as described in part in our previous papers in this series. The long-slit measurements of gas kinematics can be used to measure or place limits on the mass of a central black hole (Sarzi et al. 2001, 2002). The spectra, coupled with *HST* imaging, can be used further to probe the structure of nuclear gas disks, which we find to be influenced in many cases by nongravitational effects (Ho et al. 2002). The use of small apertures is very helpful in isolating nuclear-emission components that are lost in the contamination by circumnuclear sources, as demonstrated by our discovery of unusual broad-line emission in two galaxies (Shields et al. 2000; Ho et al. 2000). Small apertures are also important for obtaining a description of the stellar population and star formation history within the central tens of parsecs (Sarzi et al. 2005).

In the current paper we present a summary description of the SUNNS experimental design, and focus on new results for the nuclear emission-line characteristics of the sample. The spatial distribution and excitation properties of nebular emission can be used to draw conclusions about the dominant energy sources in galaxy centers, and as part of our investigation we explore the significance of aperture effects in determining the spectroscopic appearance of galaxy nuclei. Understanding the energetics of emission-line nuclei is of fundamental importance for tracing rates of star formation and black hole growth in these low-power,

[1] Based on observations with the NASA/ESA *Hubble Space Telescope* obtained at the Space Telescope Science Institute, which is operated by the Association of Universities for Research in Astronomy, Inc., under NASA contract NAS5-26555.
[2] Physics and Astronomy Department, Ohio University, Athens, OH.
[3] Max-Planck-Institut für Astronomie, Heidelberg, Germany.
[4] Centre for Astrophysics Research, University of Hertfordshire, Hatfield, UK.
[5] Physics and Astronomy Department, University of California, Irvine, CA.
[6] Astronomy Department, University of California, Berkeley, CA.
[7] Observatories of the Carnegie Institution of Washington, Pasadena, CA.
[8] Astronomy Department, University of Massachusetts, Amherst, MA.
[9] National Optical Astronomy Observatory, Tucson, AZ.
[10] Goldberg Fellow.
[11] Astronomy Department, California Institute of Technology, Pasadena, CA.

but nearly ubiquitous, objects. The data reported here also provide an improved basis for comparing energetic phenomena and structure in the Milky Way's nucleus with the centers of other similar galaxies.

2. OBSERVATIONS AND MEASUREMENTS

HST observations (GO-7361) were obtained for 24 galaxies within 17 Mpc of the Milky Way, drawn from the Palomar spectroscopic survey of nearby galaxies (Filippenko & Sargent 1985; Ho et al. 1997a). The sample was chosen to be distance-limited to maximize spatial resolution, and was selected to have nebular emission potentially suitable for kinematic studies and energetic probes. We focused our study on disk galaxies, since these objects most commonly show nebular emission in their centers. We restricted the sample to Hubble types S0–Sbc, since the nuclei of later types are more likely to be weakly defined, affected by dust, or otherwise subject to confusion. The sample was limited to galaxies with inclinations $i < 60^\circ$ to minimize extinction by dust residing in the disk. We selected objects with Hα or [N II] λ6583 line emission $\gtrsim 10^{-15}$ ergs s^{-1} cm^{-2} within a $2'' \times 4''$ aperture (from Ho et al. 1997a), with spectroscopic classifications fairly evenly distributed among Seyfert, LINER 1, LINER 2, LINER/H II "transition," and H II categories. The result is listed in Table 1.

Data were acquired in 1998 and 1999 with the Space Telescope Imaging Spectrograph (STIS) on board *HST*, using the $0.2'' \times 50''$ aperture. For each galaxy, acquisition images were obtained using the F28X50LP long-pass filter with 30 s integration, and peak-up exposures were taken in order to center the spectrograph slit on the target nucleus. Inspection of these and other archival *HST* images indicates that in all but one case, the aperture was well centered on an obvious brightness peak at the morphological center, with no indication of confusion by dust obscuration or other structures; errors in aperture centering due to dust effects are $\lesssim 0.25$ pixels $\approx 0.012''$. The exception occurred in NGC 4138, where the peak-up procedure positioned the slit on a bright foreground star offset $\sim 3.8''$ from the nucleus; we consequently dropped this object from our analysis. The slit position angle (P.A.) was left unconstrained, and thus was set by the spacecraft roll angle at the time of observation. For a given galaxy, all exposures were obtained at a single P.A.

Two-dimensional (2D) spectra were obtained with the G430L and G750M gratings, yielding spectra spanning 3300–5700 and 6300–6850 Å, with FWHM spectral resolution for extended sources of 10.9 and 2.2 Å, respectively. These intervals were chosen in order to include prominent emission lines, and to measure continuum intervals diagnostic of stellar populations and possible active galactic nucleus (AGN) contributions. The medium-resolution grating was selected for the red setting so as to enable high-precision velocity measurements of the Hα λ6563 and [N II] $\lambda\lambda$6548, 6583 lines, which tend to be the strongest optical emission features, and hence optimal for kinematic studies. Two exposures totaling $\sim$1800 s and three exposures totaling $\sim$2700 s were obtained with the blue and red settings, respectively. For most of the target galaxies, the telescope pointing was adjusted between duplicate exposures, so as to shift the location of the nucleus along the slit by increments of several pixels, to facilitate removal of hot pixels.

The resulting data were calibrated using standard methods. The 2D spectra were bias- and dark-subtracted, flat-fielded, aligned, and combined into single frames. Cosmic rays and hot pixels remaining in the combined 2D spectra were cleaned according to the prescription of Rudnick et al. (2000), and the spectra were then corrected for geometrical distortion and wavelength and flux calibrated with standard STSDAS procedures within IRAF.[12] During each reduction step, care was taken to correctly propagate the information contained in the error array corresponding to each galaxy 2D spectrum and initially provided by the STIS pipeline.

TABLE 1
GALAXY SAMPLE

Name	Distance[a] (Mpc)	Hubble Type[b]	Ground-based Spectral Class[c]
NGC 278	11.8	SAB(rs)b	H
NGC 2787	13.0	SB(r)0+	L1.9
NGC 3351	8.1	SB(r)b	H
NGC 3368	8.1	SAB(rs)ab	L2
NGC 3489	6.4	SAB(rs)0+	T2/S2
NGC 3982	17.0	SAB(r)b:	S1.9
NGC 3992	17.0	SB(rs)bc	T2:
NGC 4138[d]	17.0	SA(r)0+	S1.9
NGC 4143	17.0	SAB(s)0	L1.9
NGC 4203	9.7	SAB0−:	L1.9
NGC 4245	9.7	SB(r)0/a:	H
NGC 4314	9.7	SB(rs)a	L2
NGC 4321	16.8	SAB(s)bc	T2
NGC 4380	16.8	SA(rs)b?	H
NGC 4435	16.8	SB(s)0	T2/H:
NGC 4450	16.8	SA(s)ab	L1.9
NGC 4459	16.8	SA(r)0+	T2:
NGC 4477	16.8	SB(s)0?	S2
NGC 4501	16.8	SA(rs)b	S2
NGC 4548	16.8	SB(rs)b	L2
NGC 4596	16.8	SB(r)0+	L2::
NGC 4698	16.8	SA(s)ab	S2
NGC 4800	15.2	SA(rs)b	H
NGC 5055	7.2	SA(rs)bc	T2

[a] From Tully (1988).
[b] From de Vaucouleurs et al. (1991).
[c] From Ho et al. (1997a). For sources with two possible classifications, the first listed class is marginally preferred, and adopted here when objects are sorted by type. Colons and double colons indicate uncertain and highly uncertain classifications, respectively.
[d] Due to a pointing error during the observations of NGC 4138, this galaxy was dropped from the analysis.

To represent the nuclear spectrum of each galaxy, we extracted aperture spectra 5 pixels wide ($\sim 0.25''$), centered on the brightest part of the continuum, using the IRAF task APALL. The extracted spectra thus consist of the central emission convolved with the STIS spatial point-spread function and sampled over an aperture of $0.25'' \times 0.2''$, roughly corresponding to a circular aperture with radius $R = 0.13''$, or 8.2 pc for the mean sample distance of $\sim$13 Mpc (or $R = 4$–11 pc for the full range of galaxy distances). In addition, from the 2D error array corresponding to each 2D spectrum, we extracted the central five 1 pixel wide aperture spectra, and added them quadratically to obtain the error array corresponding to each nuclear extraction. The resulting 1D spectra for the blue (G430L) setting appear in Sarzi et al. (2005), while those for the red (G750M) setting are shown here in Figure 1.

The emission-line equivalent widths in the nuclear spectra are often small, and consequently require subtraction of the underlying starlight in order to measure accurate emission-line fluxes. We modeled the continuum with linear combinations of stellar spectra from the MILES library of Sanchez-Blazquez et al. (2006), with weights and velocity broadening optimized with the

[12] IRAF is distributed by the National Optical Astronomical Observatory, which is operated by AURA, Inc., under contract to the NSF.

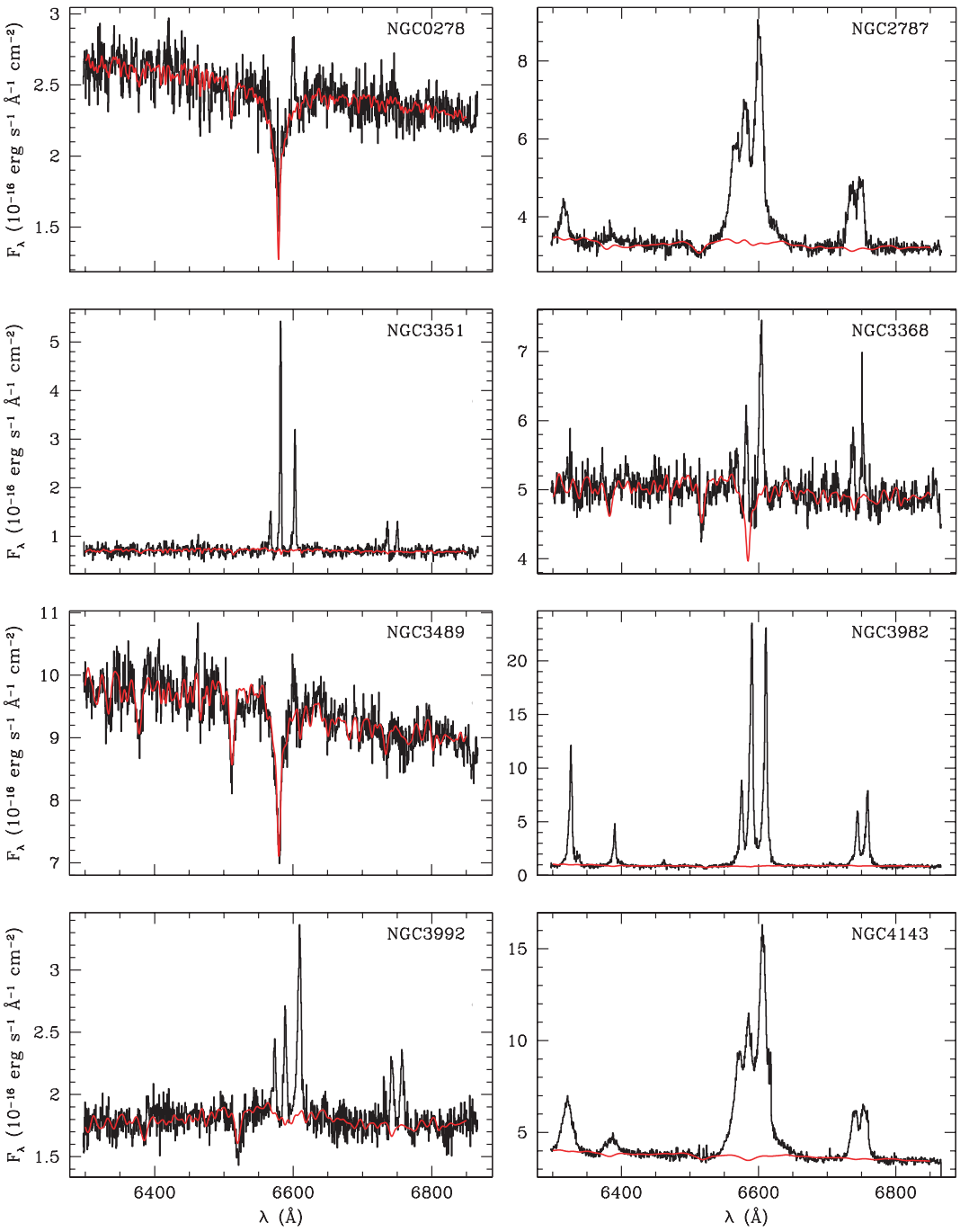

FIG. 1.— Spectra of the sample galaxy nuclei acquired with the G750M grating, as a function of observed wavelength (*black lines*), with fits to the stellar continuum overplotted (*red lines*).

direct-fitting method described in Sarzi et al. (2006). This is similar to the method of Rix & White (1992), except that the spectral regions affected by nebular emission are no longer excluded from the fitting process, since the emission lines are treated as Gaussian templates and fitted simultaneously with the stellar templates to the observed spectra. This has the advantage of maximizing the spectral information available to the fitting algorithm.

As the blue and red spectra have different spectral resolutions, they cannot be fitted simultaneously. On the other hand, the presence of stronger emission lines and the limited number of absorption features makes it difficult to independently match the stellar continuum of the red bandpass. We therefore fit first the blue spectra, which are important for constraining the mix of template stellar types, and use the resulting optimal combination of templates to match the red spectra, allowing only for a different velocity broadening. The fitting of the blue spectra includes reddening due to interstellar dust, both in the Milky Way and in the sample galaxies, and due to dust in the emission-line regions. The latter affects only the fluxes of the emission-line templates, and is constrained by the expected decrement of the Balmer lines. In matching the blue spectra we imposed the same kinematics for both forbidden and recombination lines. We also restricted the stellar template library to spectra with values for the Hβ absorption line strength index exceeding 0.1 Å.

In the present study we are interested in obtaining the best empirical fit to the starlight, and no a priori assumptions are made

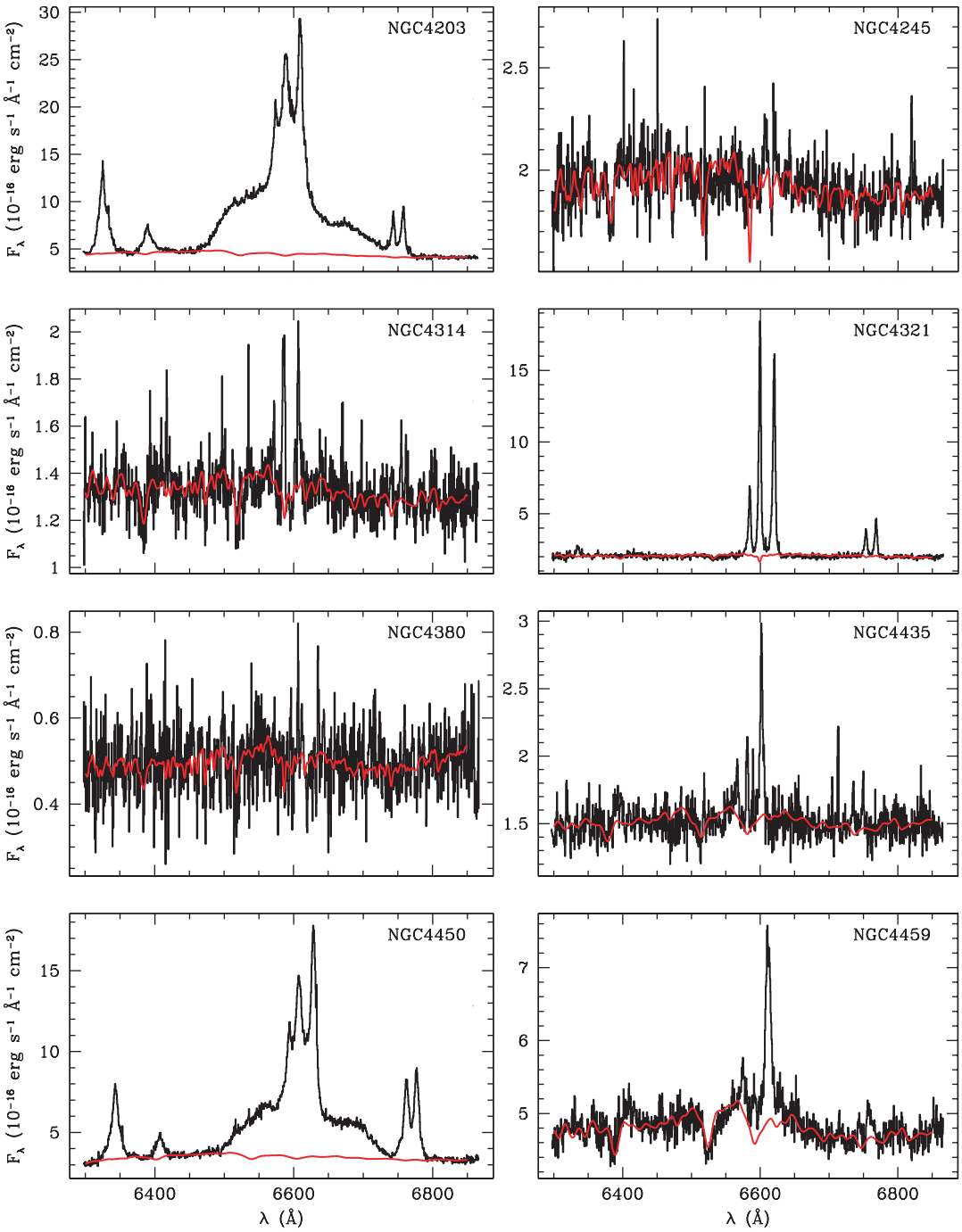

FIG. 1.—*Continued*

concerning the relative weighting of different stellar types; our method here consequently differs somewhat from that employed in our population analysis (Sarzi et al. 2005), which is based on templates corresponding to parameterized star formation histories. The fits to the blue spectra are very similar to the parameterized fits plotted in Sarzi et al. (2005), although the MILES spectra can match several spectral regions where models such as those of Bruzual & Charlot (2003) would need to account for nonsolar abundance of α-elements before they could match the data.

The best description for the stellar continuum in the red bandpass is overplotted on the spectra shown in Figure 1. The fits for the red spectra differ from those for the blue bandpass not only in that they use a different velocity broadening and the optimal combination of templates from the fit on the blue spectra, but also in that they employ a generalized multiplicative second-order polynomial adjustment instead of a specific dust-reddening law. Emission-line templates were also used while fitting the red spectra, although for galaxies with complex line profiles or broad components the regions affected by emission were simply excluded from the fit.

For many of our target objects, the emission lines within the nuclear aperture are weak. We attempted to measure lines that were visible in much of the sample on inspection, or likely to be present based on the behavior of line-intensity ratios in other nebular sources. Specifically, we measured or placed limits on the flux in [O II] λ3727, Hγ λ4340, Hβ λ4861, [O III] $\lambda\lambda$4959,

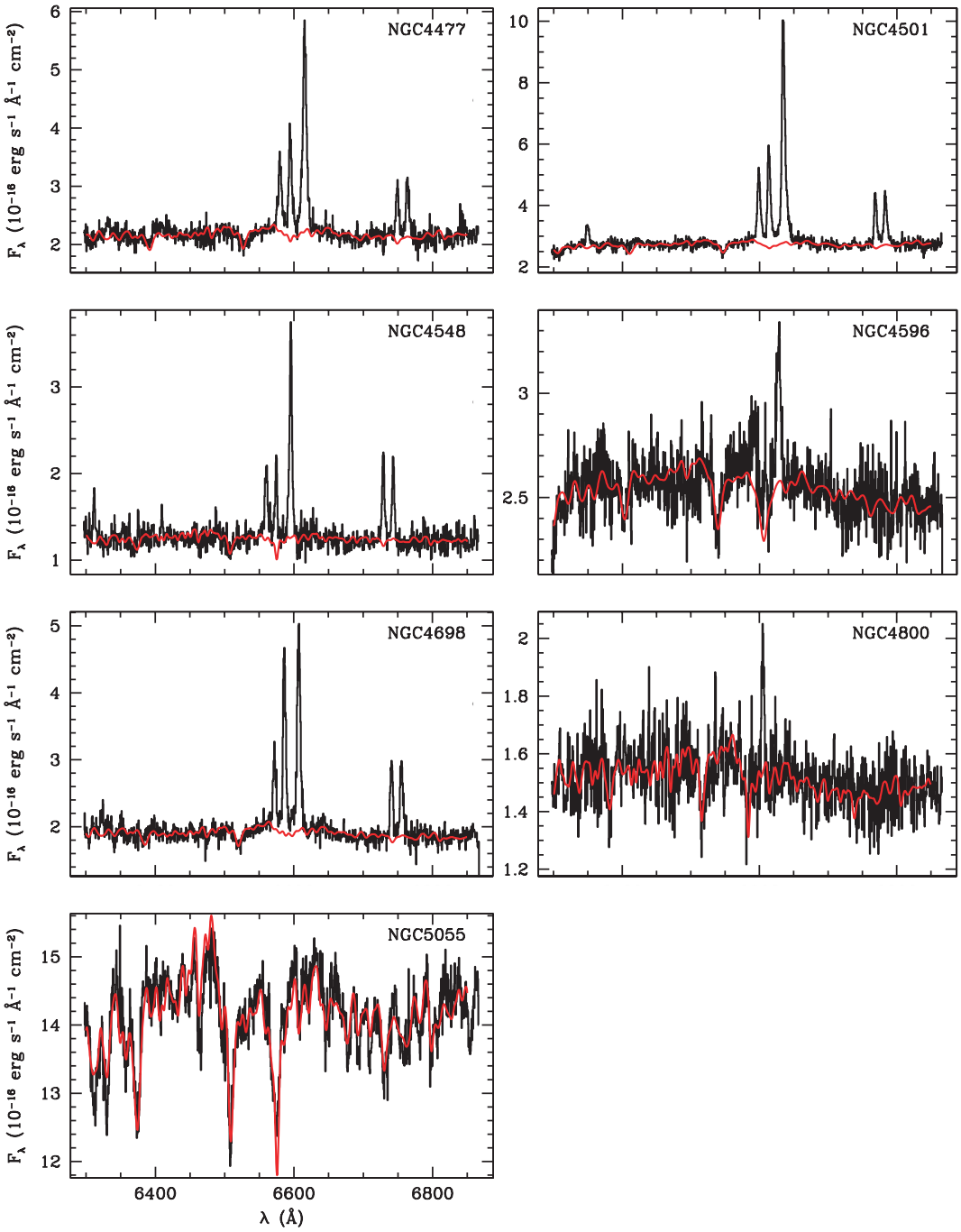

FIG. 1.—*Continued*

5007, [O I] λ6300, [N II] $\lambda\lambda$6548, 6583, Hα λ6563, and [S II] $\lambda\lambda$6716, 6731. The lines were measured from the starlight-subtracted spectra using SPECFIT (Kriss 1994), as implemented in IRAF. This routine is suitable for fitting complicated line profiles with additional constraints between lines, while also generating error estimates for measured quantities. Gaussian profiles were assumed for the lines; a few sources required double Gaussians to obtain a good match to the observed lines, and additional components were included in cases where there was evidence of broad Balmer emission (§ 3.3).

To improve the fitting accuracy, we introduced constraints to reduce the number of fit parameters when justified by physical arguments or by our previous experience with ground-based spectra (e.g., Ho et al. 1997a). The Hα, [N II], and [S II] lines were assumed to share a common centroid velocity, and the [N II] and [S II] lines were assumed to share a common velocity width. A flux ratio of 1:3 was assumed for the [N II] $\lambda\lambda$6548, 6583 and [O III] $\lambda\lambda$4959, 5007 doublets, as dictated by atomic physics (e.g., Osterbrock 1989). The Hβ and Hγ lines were also assumed to share a common velocity and profile. The G430L and G750M spectra were fit separately because of their differing spectral resolution and possible zero-point wavelength offsets. In determining relative wavelengths for lines with shared velocities, rest wavelengths to six significant figures were taken from Kaufman & Sugar (1986) for the forbidden lines, and from Wiese et al. (1966) for the Balmer lines. The resulting line fluxes are listed in Table 2.

TABLE 2
NARROW EMISSION LINE MEASUREMENTS

Galaxy Name (1)	[O II] λ3727 (2)	Hγ (3)	Hβ (4)	[O III] λ5007 (5)	[O I] λ6300 (6)	Hα (7)	[N II] λ6583 (8)	[S II] λ6716 (9)	[S II] λ6731 (10)	EW(Hα) (Å) (11)
NGC 278.....	<23	<23	<23	<23	<25	<25	<25	<25	<25	<1.0
NGC 2787[a]	390 ± 40	106 ± 11	200 ± 20	280 ± 30	118 ± 12	180 ± 20	500 ± 50	200 ± 20	210 ± 20	6.3 ± 0.9
NGC 3351.....	<9	<9	22 ± 3	25 ± 3	<54	126 ± 13	71 ± 7	<18	<18	19 ± 3
NGC 3368.....	67 ± 11	<32	<32	<32	<34	117 ± 12	139 ± 14	59 ± 11	59 ± 11	1.7 ± 0.2
NGC 3489.....	<39	<39	<39	<39	<57	<57	<57	<57	<57	<0.6
NGC 3982.....	560 ± 60	130 ± 15	240 ± 40	5000 ± 500	620 ± 60	1400 ± 140	1380 ± 140	310 ± 30	460 ± 50	180 ± 20
NGC 3992.....	61 ± 6	12 ± 4	<11	36 ± 4	<18	44 ± 6	87 ± 9	37 ± 6	32 ± 6	3.0 ± 0.4
NGC 4143[a]	690 ± 70	<170	400 ± 40	900 ± 90	750 ± 70	390 ± 40	1070 ± 110	340 ± 30	340 ± 30	11 ± 2
NGC 4203[a]	950 ± 100	450 ± 40	900 ± 90	1700 ± 170	1070 ± 110	450 ± 40	1080 ± 110	250 ± 30	340 ± 30	10 ± 1
NGC 4245.....	<15	<15	<15	<15	<28	<28	<28	<28	<28	<1.2
NGC 4314.....	<13	<13	<13	<13	<22	32 ± 7	<22	<22	<22	2.5 ± 0.6
NGC 4321.....	100 ± 10	53 ± 6	140 ± 14	47 ± 6	106 ± 13	740 ± 70	700 ± 70	112 ± 11	132 ± 13	37 ± 5
NGC 4380.....	<9	<9	<9	<9	<15	<15	<15	<15	<15	<2.5
NGC 4435.....	<14	<14	<14	<14	<22	28 ± 7	63 ± 7	<22	<22	1.9 ± 0.4
NGC 4450[a]	800 ± 80	220 ± 20	400 ± 40	800 ± 80	500 ± 50	400 ± 40	770 ± 80	420 ± 40	460 ± 50	12 ± 2
NGC 4459.....	42 ± 7	<22	<22	27 ± 7	<36	63 ± 12	250 ± 20	<36	38 ± 12	1.4 ± 0.2
NGC 4477.....	86 ± 9	14 ± 4	28 ± 4	82 ± 8	26 ± 9	110 ± 11	240 ± 20	62 ± 9	62 ± 9	5.6 ± 0.8
NGC 4501.....	98 ± 10	<14	36 ± 5	163 ± 16	54 ± 9	152 ± 15	360 ± 40	96 ± 10	92 ± 9	5.7 ± 1.1
NGC 4548.....	55 ± 6	<10	<10	37 ± 4	23 ± 7	48 ± 7	110 ± 11	48 ± 7	40 ± 7	3.2 ± 0.5
NGC 4596.....	<15	<15	<15	<15	<23	25 ± 8	69 ± 8	<23	<23	<0.7
NGC 4698.....	90 ± 9	40 ± 5	60 ± 6	149 ± 15	<39	150 ± 15	200 ± 20	60 ± 6	70 ± 7	8.9 ± 1.3
NGC 4800.....	<13	<13	<13	<13	<20	<20	<20	<20	<20	<1.0
NGC 5055.....	<76	<76	<76	<76	<71	<71	<71	<71	<71	<0.6

NOTES.—Col. (1): Galaxy name. Cols. (2)–(10): Narrow-line fluxes in units of 10^{-17} ergs s^{-1} cm^{-2}; upper limits are 3 σ. Col. (11): Equivalent width of narrow Hα.
[a] See § 3.3 for discussion of systematic errors in Hα fluxes for these sources.

The line fluxes are uncertain due to both statistical fluctuations and systematic errors. SPECFIT uses a χ^2-minimization algorithm, which provides one estimate of the line flux uncertainties. As a measure of the possible systematic error, we also calculated an equivalent 1 σ Gaussian uncertainty based on the standard deviation σ_c per pixel in the residual continuum after starlight subtraction. The standard deviation was computed in regions devoid of emission lines and traces structure due to imperfect continuum subtraction, in addition to statistical fluctuations. The corresponding error is then given by a Gaussian profile with amplitude of 1 σ_c, and a width typical of the measured narrow lines (FWHM of 300 km s^{-1} for G750M and 550 km s^{-1} for G430L, where the width includes instrumental broadening). In determining a final value for the flux uncertainty, we adopted the largest of (1) the SPECFIT error, (2) the Gaussian 1 σ uncertainty, and (3) a conservative minimum error of 10% of the line flux. As a consistency test, we repeated the line measurements after subtracting the best-fit multi-age stellar population models for these spectra that are described by Sarzi et al. (2005). Line fluxes were measured from the continuum-subtracted spectra by direct integration over the line profile, using SPLOT in IRAF. The results showed good consistency within the measurement uncertainties with the values listed in Table 2.

3. RESULTS

The *HST* aperture employed for this study is much smaller than typical ground-based apertures, and a comparison of nebular properties as seen on these different scales provides useful information on the structure of emission nuclei. The Palomar spectra used to define the current sample employed a $2'' \times 4''$ aperture, which is ∼10 times larger in linear dimension and 160 times larger in area than the SUNNS nuclear aperture. The linear scales probed by these data are ∼100 versus ∼10 pc.

3.1. *Spatial Extent of Emission*

The degree to which the nebular emission in our sample galaxies is centrally concentrated can be gauged from a comparison of fluxes measured through the SUNNS and Palomar apertures. The result is shown in Figure 2, which displays the ratio of narrow Hα fluxes as a function of Palomar spectroscopic class. The sequence of categories on the abscissa is intended to reflect the degree to which the nuclei show evidence of being powered

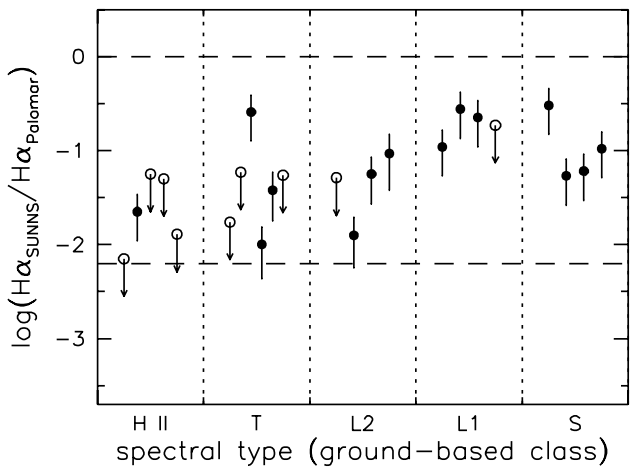

FIG. 2.—Ratio of narrow Hα flux measured in the SUNNS data relative to that measured at Palomar, as a function of spectroscopic class as determined from the Palomar spectra (T = H II/LINER transition source, L2 = LINER 2, L1 = LINER 1.9, S = Seyfert 1.9 or 2). Upper limits are represented by open symbols. The upper dashed line represents a unit flux ratio, and the lower dashed line represents the value predicted from the ratio of aperture areas, for a source with uniform surface brightness.

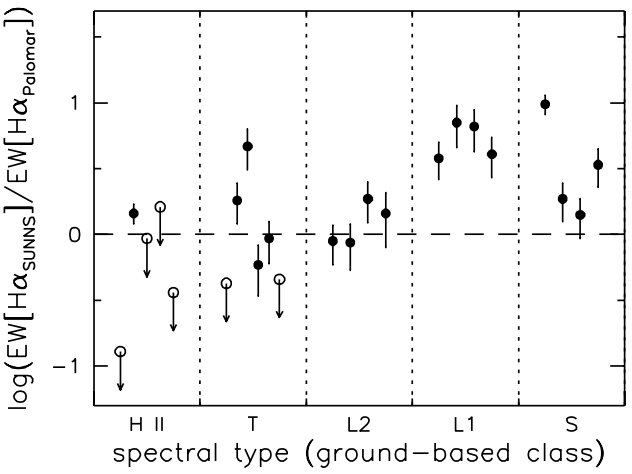

FIG. 3.—Ratio of narrow Hα equivalent width measured in the SUNNS data relative to that measured at Palomar (Ho et al. 1997a) as a function of spectroscopic class as determined from the Palomar spectra. Upper limits are represented by open symbols.

by accretion. In this and subsequent figures displaying ratios, the plotted error bars are propagated from the uncertainties listed in Table 2 for the SUNNS measurements and in Ho et al. (1997a) for the Palomar data. For a uniform nebular surface brightness, the flux ratio should be −2.2 dex. In the majority of cases the ratio is measured to be higher, indicating some degree of central concentration. On the other hand, for all of the galaxies, the small-aperture measurement shows a significant reduction in flux relative to the Palomar value, indicating that the central nebulae in these objects are resolved at *HST* resolution.

Figure 2 shows evidence of a trend in that sources showing the strongest indications of accretion power (LINER 1s and Seyferts) display the largest ratios, implying greater concentration. In contrast, the H II nuclei show the smallest ratios, and in fact four of the five H II nuclei are undetected in Hα in the SUNNS aperture. The star formation powering H II "nuclei" apparently resides on scales of tens of parsecs or more (see, e.g., Hughes et al. [2003], Cid Fernandes et al. [2004], and González Delgado et al. [2004] for related results). The narrow emission-line equivalent widths (EWs; see Table 2 and Fig. 3) show a similar trend,[13] with larger EW(Hα) found in the SUNNS aperture for the LINER 1 and Seyfert nuclei, but smaller EW(Hα) in the small aperture for the majority of H II, transition, and LINER 2 nuclei.

3.2. *Emission Line Ratios*

While a direct measurement of line ratio gradients is possible in principle from the *HST* long-slit data, in practice the signal-to-noise ratio severely hampers detailed study of spatial variations.

[13] Error bars in Fig. 3 are smaller in some cases than in Fig. 2 because the equivalent widths are insensitive to absolute flux calibration uncertainties in the Palomar spectra.

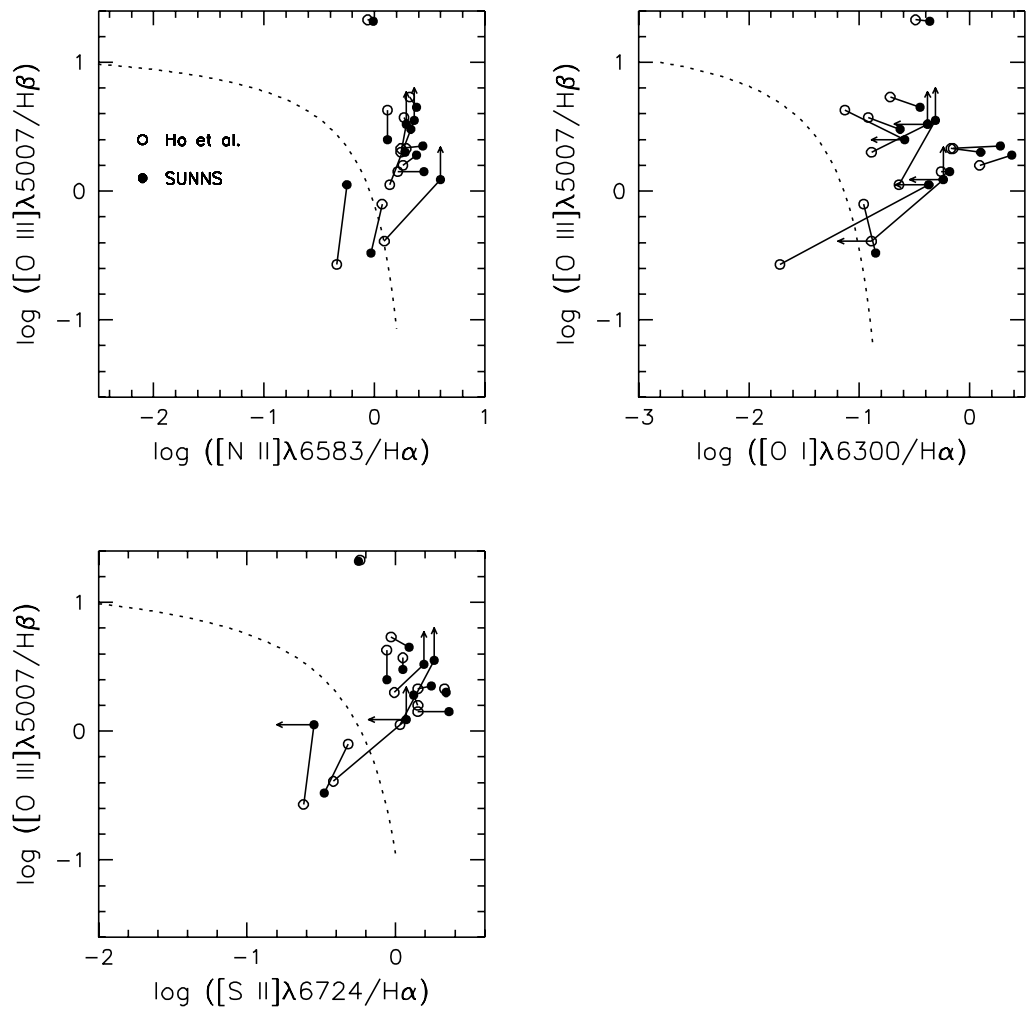

FIG. 4.—Emission line intensity ratios as measured through the large Palomar aperture (Ho et al. 1997a) and by SUNNS. The dotted line is the boundary between starburst and nonstarburst sources given by Kewley et al. (2001). [S II] λ6724 represents the sum of [S II] $\lambda\lambda$6716, 6731.

Comparison of line ratios measured in the SUNNS and Palomar apertures provides an alternative means of quantifying excitation gradients. In addition to yielding ~10 times more signal, the Palomar aperture avoids possible problems with azimuthal variations in extended emission that are not adequately sampled by the narrow SUNNS slit. Line ratios useful as diagnostics that are also measured for a significant number of sample members are limited, but four particularly relevant ratios are [O III] λ5007/Hβ, [O I] λ6300/Hα, [N II] λ6583/Hα, and [S II] $\lambda\lambda$6716, 6731/Hα. These diagnostics are commonly employed in classification of nebular sources (e.g., Veilleux & Osterbrock 1987), and standard diagrams used for this purpose are shown in Figure 4, with measurements from both Palomar and SUNNS plotted.

There is considerable variation in the behavior of different objects in Figure 4, but several conclusions can nonetheless be drawn from these plots. First, the line ratios are often rather insensitive to aperture size, and in the present comparison show changes that are usually less than a factor of 2. Related to this, the sources generally do not shift their positions by large amounts in the line ratio diagrams, which means that their classification is insensitive to aperture size. This finding has interesting and important implications that we examine in detail below. One limitation of the 2D line ratio diagrams is that the SUNNS observations provide only upper limits for both [O III] and Hβ for nearly half the sample, thus preventing their inclusion in Figure 4. An alternative is to compare line intensity ratios individually, and for this purpose we plot in Figure 5 the "ratio of ratios" for the measurements obtained in the two apertures.

Several patterns are discernible in Figure 5. [O I]/Hα is arguably the best indicator of excitation beyond the contributions of normal H II regions, since it requires a significant partially ionized zone for its production. The [O I] line is in fact most significant in the LINER 1 and Seyfert nuclei, and Figure 5 shows a clear tendency for the ratio to be larger in the small aperture for these sources. A weaker trend in the same direction exists for [N II]/Hα, but no trend is evident for [S II]/Hα. The more limited measurements of [O III]/Hβ show little dependence on aperture size, except for some tendency for the ratio to decrease in the small aperture in the Seyfert nuclei.

Density gradients may be a factor in the nebular emission structure reflected in Figure 5. Previous studies have shown indirect evidence from line width–critical density correlations (e.g., Pelat et al. 1981; Filippenko & Halpern 1984), as well as direct evidence from the [S II] density diagnostic (Barth et al. 2001) that densities increase toward small radii in the narrow-line regions of AGNs. Figure 6 shows the density-sensitive [S II] λ6716/λ6731 line ratio for the sample sources, as measured in both the Palomar and SUNNS spectra. The ratio is lower in all but one case for the small aperture measurement, implicating a characteristically higher density on smaller radial scales; median values are 1.2 from the Palomar measurements and 0.95 from SUNNS, corresponding to densities of ~200 and ~700 cm^{-3}, respectively. These values are presumably emissivity-weighted averages of a potentially much broader span of densities. The different spectral classes show substantial overlap in their distributions in Figure 6.

The different behavior observed in the [O I], [N II], and [S II] lines in Figure 5 can potentially be understood as a consequence of the varied critical densities for the forbidden lines. In the SUNNS aperture, a significant fraction of the nebular gas for the LINERs and Seyferts evidently has a density similar to or greater than the [S II] $\lambda\lambda$6716, 6731 critical densities $n_{\rm crit}$ of $\sim 1.5 \times 10^3$ and $\sim 3.9 \times 10^3$ cm^{-3} (e.g., Peterson 1997), which could act to depress the [S II]/Hα ratio in the small aperture. The [S II] $n_{\rm crit}$ values are the lowest of those for the lines shown in Figure 5. In

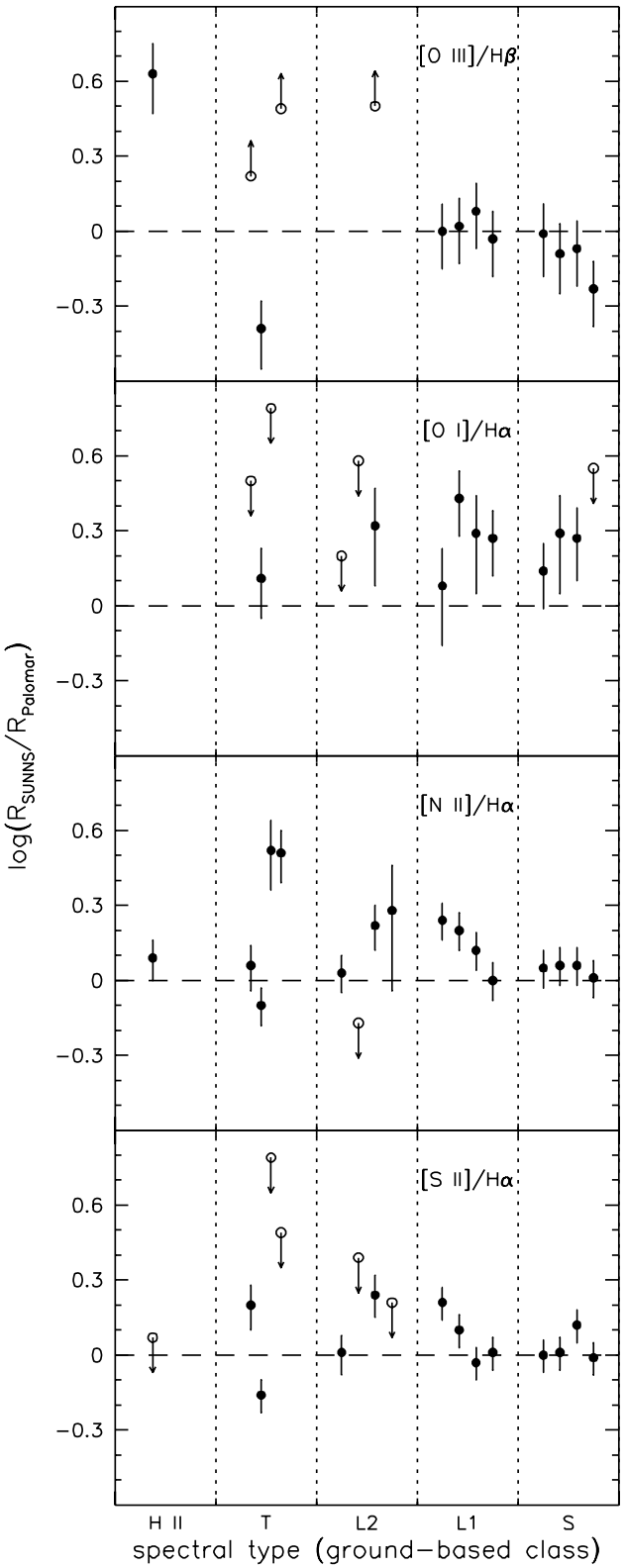

FIG. 5.—SUNNS/Palomar ratios of the indicated diagnostic flux ratios, as a function of spectroscopic class. Limits are represented by open symbols. Points for a given source have a common horizontal location (offset for clarity) within the classification bins in all plots shown in Figs. 2, 3, and 5.

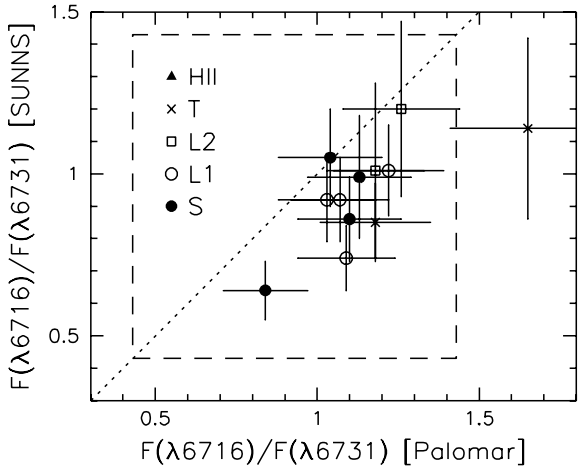

FIG. 6.—Line flux ratio [S II] λ6716/[S II] λ6731 as measured by SUNNS vs. Palomar. The dotted line represents $x = y$ and the dashed box outlines the boundary of allowed values predicted from theory, defined by the high- and low-density limits. The data reveal a strong trend of lower ratios, and hence higher average densities, in the SUNNS aperture.

contrast, [O I] λ6300, with $n_{\rm crit} \approx 1.8 \times 10^6$ cm^{-3}, remains strong in the small aperture; the larger [O I]/Hα ratios found with SUNNS may reflect an increased importance of partially ionized gas on small scales, but would also be consistent with a higher nebular temperature in dense regions in which cooling by low-$n_{\rm crit}$ emission (e.g., from infrared fine-structure lines) is inefficient. [N II] λ6583, with an intermediate $n_{\rm crit}$ value of $\sim 8.7 \times 10^4$ cm^{-3}, shows a weaker trend in the same direction. The overall results suggest that a significant fraction of the nebular gas in galaxies on scales of $\sim$10 pc has densities of $\sim 10^4$ cm^{-3}. The [O III] λ5007 line, with $n_{\rm crit} \approx 7 \times 10^5$ cm^{-3}, does not readily fit into this scenario. For the Seyfert nuclei in particular, the [O III]/Hβ ratio tends to decrease in the small aperture, and there is some degree of negative correlation between the [O III]/Hβ and [O I]/Hα ratios, suggesting that ionization structure—which will be sensitive to ionization parameter and hence the detailed radial variation in density—also plays a role in the aperture dependence.

3.3. *Broad Lines*

The existing Palomar observations provided evidence that six of our 23 target galaxies exhibit weak quasar-like broad Hα emission, resulting in classification as LINER 1.9 (NGC 2787, NGC 4143, NGC 4203, and NGC 4450) or Seyfert 1.9 (NGC 3982, and NGC 4501) nuclei (Ho et al. 1997c). We investigated whether a broad component was also present in the *HST* spectra for these sources and the other objects in our sample. The SUNNS data for two of the LINER 1.9 galaxies, NGC 4203 and NGC 4450, display evidence of not only a Gaussian broad Hα line, as seen from the ground, but also a very broad, double-shouldered component (see Fig. 1); these findings are discussed in detail elsewhere (Shields et al. 2000; Ho et al. 2000). We attribute the discovery of the additional broad features to the improved contrast in the small *HST* aperture between the broad emission, which presumably arises within $\lesssim$1 pc of the center, and the stellar continuum plus narrow-line emission, which is more widely dispersed in origin. The implication is that such broad emission may be common in low-luminosity AGNs, and a signature of the accretion structure in low accretion-rate nuclei. Other examples of double-shouldered emission profiles found in *HST* spectra of LINER 1 nuclei are described by Bower et al. (1996) and Barth et al. (2001).

Figure 7 shows the results of a profile decomposition using the SUNNS data for the remaining four galaxies in which broad emission was previously suspected. A common profile shape was employed to represent the [N II], narrow Hα, and [S II] lines; double Gaussians were adopted to better match the profiles for NGC 3982 and NGC 4143. An additional broad Hα component with unconstrained width and central wavelength was included in the fit. Strong evidence for a broad emission feature is found in NGC 2787 and NGC 4143, while marginal evidence for such emission is present in NGC 4501, and a reasonable fit for NGC 3982 can be obtained with no broad component. The narrow-line fluxes resulting from this decomposition are listed in Table 2; broad-line fluxes and the fraction $f_{\rm blend}$ of the total Hα + [N II] complex represented by the broad Hα feature are listed in Table 3, along with the corresponding numbers measured in the Palomar spectra. For the four galaxies where broad emission appears to be confirmed (NGC 2787, NGC 4143, NGC 4203, and NGC 4450),

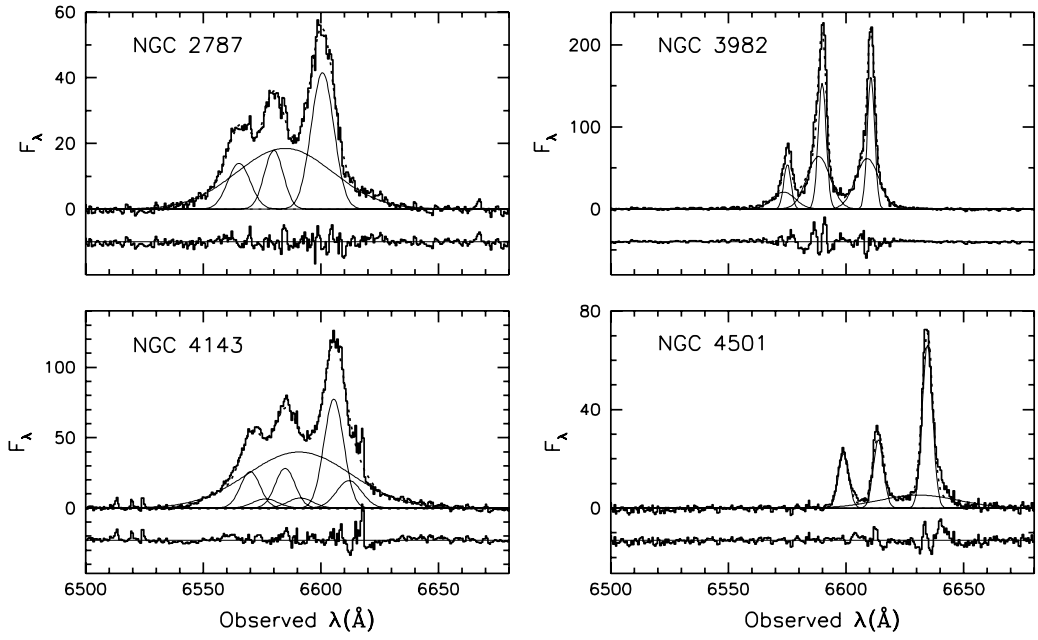

FIG. 7.—Continuum-subtracted spectra in the Hα + [N II] region, plotted with Gaussian model components (*solid curves*), the reconstructed blend (*dotted lines*), and residuals (offset vertically for better visibility).

TABLE 3
BROAD Hα PROPERTIES

GALAXY	PALOMAR MEASUREMENT[a]		SUNNS MEASUREMENT[b]	
	log F(Hα)	$f_{\rm blend}$	log F(Hα)	$f_{\rm blend}$
NGC 2787.....	−13.55	0.35	≤−14.02	≤0.53
NGC 3982.....	−13.85	0.12	≤−15.05	≤0.03
NGC 4143.....	−13.41	0.45	≤−13.66	≤0.55
NGC 4203[c]	−13.46	0.34	≤−13.54 (−12.83)	≤0.61 (0.89)
NGC 4450[c]	...	0.20	≤−14.00 (−13.20)	≤0.41 (0.82)
NGC 4501.....	−14.02	0.09	−14.66	0.26

NOTES.—Fluxes are in units of ergs s^{-1} cm^{-2} and are not corrected for extinction. The quantity $f_{\rm blend}$ is the fraction of the total Hα+[N II] flux contributed by the broad Hα feature.

[a] From Ho et al. (1997c).

[b] Upper limits reflect possible systematic uncertainties in profile decomposition (§ 3.3). Uncertainty in the SUNNS measurement for NGC 4501 is ∼100%.

[c] Fluxes for "normal" Gaussian component as reported by Ho et al. (1997a). Additional, very broad components were detected in the SUNNS spectra, and results with this component included are listed in parentheses; see Shields et al. (2000; NGC 4203) and Ho et al. (2000; NGC 4450).

$f_{\rm blend}$ increases if these values are taken at face value, as expected if the narrow emission is resolved and diminished in the small aperture while the broad emission remains unaffected by slit losses.

Closer scrutiny of the deblending results suggests a problem with the fitting procedure, however. The values listed in Table 2 imply Hα/Hβ ratios for the narrow component of 0.9 ± 0.1, 1.0 ± 0.1, 0.50 ± 0.07, and 1.0 ± 0.1 for NGC 2787, NGC 4143, NGC 4203, and NGC 4450, respectively. These ratios are considerably smaller than the theoretical ratio of 3.1 predicted for AGN narrow-line regions (Osterbrock 1989), and are impossible to understand on physical grounds. The low values are unlikely to be caused by broad-line contamination of Hβ; NGC 4203 and NGC 4450 both show evidence of broad emission in Hβ and Hγ, but this component is included as a separate component when determining the narrow Balmer fluxes. No evidence of broad emission is seen in these lines for NGC 2787 and NGC 4143. The narrow Hγ/Hβ ratios are, moreover, normal: NGC 2787, NGC 4143, NGC 4203, and NGC 4450 display Hγ/Hβ = 0.53 ± 0.07, <0.43, 0.50 ± 0.07, and 0.55 ± 0.08, respectively, in reasonable agreement with the predicted recombination value of ∼0.47. There is no evidence of significant discontinuities between the G430L and G750M spectra indicative of flux calibration errors; almost all of the other objects in our sample show narrow Hα/Hβ ratios consistent with the theoretical prediction (NGC 4698 has a ratio of 2.5 ± 0.4), or a larger ratio attributable to reddening. It is noteworthy that for the four galaxies in question, the forbidden line/Hα flux ratios are unusually large for LINERs or Seyfert nuclei (although it must be kept in mind that the SUNNS aperture does not sample the full narrow-line region).

Given these findings, we strongly suspect that the deblending procedure outlined above and illustrated in Figure 7 underestimates the true narrow Hα flux, which in turn would produce an overestimate of the broad component flux. We experimented with alternative parameterizations of the fits for NGC 2787 and NGC 4143, including decoupling of the narrow Hα line widths from the other lines, forcing the narrow Hα flux to match the value predicted from Hβ, and forcing the narrow Hα width to match that of Hβ. In general, these approaches were not particularly satisfactory at matching the detailed profile structure, resulting in residuals larger than seen in Figure 7. This outcome suggests that the narrow and/or broad profiles are rather more complex than simple Gaussians and that significant differences may exist between the different narrow-line profiles. A possible broader component of [N II] than is currently represented in our deblending model may also be suggested by the redward displacement of the broad Hα feature relative to the narrow emission found in the four galaxies at issue here, since the stronger line in the doublet, λ6583, would thereby add flux that our default model would interpret as redshifted Hα emission.

We therefore caution that the fluxes of narrow Hα, and possibly [N II], in Table 2 for these objects may suffer from systematic errors in excess of the listed uncertainties. For purposes of comparison with the Palomar results, however, the fact that we employed a very similar fitting algorithm may mitigate the influence of these errors. It is noteworthy that the Palomar measurements from Ho et al. (1997a) yield Hα/Hβ ratios of 1.9, 1.6, 1.0, and 2.6 for NGC 2787, NGC 4143, NGC 4203, and NGC 4450, respectively, which likewise fall short of the recombination prediction and suggest similar systematic errors to what we have encountered with the SUNNS data. In ratioing the SUNNS measurements to the Palomar measurements (e.g., in Figs. 2, 3, and 5), we can thus expect these errors to cancel out at least partially. A best estimate of the true narrow Hα flux is probably that derived from the narrow Hβ flux, scaled by the recombination prediction, which yields $(6.2 \pm 0.6,\ 12 \pm 1,\ 28 \pm 3,\ 12 \pm 1) \times 10^{-15}$ ergs s^{-1} cm^{-2} for NGC 2787, NGC 4143, NGC 4203, and NGC 4450, respectively.

Comparison of the SUNNS broad Hα fluxes with those from Palomar reveals a surprising trend, in that the SUNNS flux is in all cases smaller. Taking the profile decomposition results at face value, the median reduction is a factor of ∼3. It is not clear how this outcome could result from systematic errors in the deblending process. We also do not expect the broad feature to suffer from aperture losses in the SUNNS data, since the emission is expected to arise from subparsec scales. For spatially unresolved sources, the STIS flux calibration corrects for aperture transmission losses to within an accuracy of ∼5% at Hα (Bohlin & Hartig 1998). The present result could be understood physically if the broad emission is variable; the sources in the Palomar survey identified as L1.9 or S1.9 nuclei would then have preferentially been in a high flux state, since sensitivity limits dictate that objects in low flux states would not be detected as broad-line objects. If the sources vary on timescales shorter than the decade interval between the Palomar and SUNNS observations, we would then expect that the broad Hα flux would be lower in a majority of cases in the second-epoch observation. We would also predict that some number of sources seen as Type 2 nuclei in the Palomar data would display new detectable broad components at the second epoch. Variability in broad-line emission would not be surprising, and has been reported in similar low-luminosity AGNs previously (e.g., Eracleous & Halpern 2001 and references therein).

For the sources in our sample that appear in the Palomar spectra as narrow-line objects, it is therefore a surprise that the *HST* spectra provide no new indications of broad Hα. This conclusion was reached after examining the residuals from fitting with purely narrow-line profiles, as described above. The lack of newly detected broad-line sources is curious with respect to the variability prediction noted above, but also given the expected increase in sensitivity in the small *HST* aperture due to the reduction in circumnuclear contamination. Investigation of a larger sample would be desirable in order to clarify the generality of this result and its implications.

4. DISCUSSION

4.1. *AGN Classification and Aperture Size*

An interesting question that can be addressed with the results of this study is the extent to which the spectroscopic classification of a galaxy nucleus depends on the measurement aperture employed. The results from § 3.1 indicate that the SUNNS aperture typically excludes most of the emission that is seen in the Palomar measurement, and that nebulosity that is clearly dominated by an accretion source tends to be the most centrally concentrated. We might therefore expect the *HST* aperture to isolate gas that is higher in excitation/ionization and more dominated by the central engine, to the extent that one is present. Likewise, the small-aperture measurement should increase the probability of detection for broad Hα components. In summary, the simple prediction from these considerations is that the SUNNS nuclear spectra should appear more AGN-like than the corresponding Palomar spectra, for nuclei in which accretion is important as a power source.

Objects of particular interest in this regard are the H II/LINER transition nuclei. These sources are intermediate in their emission properties between H II nuclei and LINERs or Seyfert nuclei (e.g., Ho et al. 1997a; Hao et al. 2005); other labels applied to such objects are "composite nuclei" (e.g., Kennicutt et al. 1989; Véron et al. 1997) and "weak [O I] LINERs" (e.g., Filippenko & Terlevich 1992). The standard interpretation for these sources, which are very common (~25% of bright galaxies; Ho et al. 1997b), is that their spectra trace a mix of AGN emission and circumnuclear H II regions. This picture is supported by kinematically distinct emission for the two components in some galaxies (Véron et al. 1997), and by aperture-dependent line ratios on kpc scales for AGNs that may reflect different admixtures of the two emission sources (Storchi-Bergmann 1991). Under this scenario, we would expect the nuclei to more strongly resemble LINERs or Seyferts in the *HST* spectra, since the small aperture should act to exclude a part of the circumnuclear nebulosity.

From the results reported in § 3, there is only limited support for these predictions. The LINER 1s and Seyfert nuclei show a modest aperture dependence in the line ratios that appears to reflect, at least partially, density effects (§ 3.2). To the extent that ionization gradients are present, it seems that the ionization often *decreases* on smaller scales. If we apply to the SUNNS measurements the same classification criteria as employed by Ho et al. (1997a) for the Palomar observations, we find that only three objects formally change their classification. NGC 3992 and NGC 4548, classified respectively as a transition object and a LINER 2 in the Palomar spectra, show higher excitation in the small aperture, with an O III/Hβ ratio consistent with a borderline Seyfert identification. Conversely, NGC 4698, with a Palomar classification as a Seyfert 2, shows a decrease in excitation in the SUNNS data consistent with classification as a LINER or transition nucleus. The composite model for transition objects is not strongly supported by these data. Approximately half of the admittedly small original sample of transition sources shows little aperture dependence in the line ratios, and in particular these objects do not appear as pure LINERs or Seyferts in the SUNNS measurement. None of the narrow-line objects reveal new evidence of broad Hα emission when viewed at *HST* resolution (see also González Delgado et al. 2004).

The behavior of the transition objects is a surprise. The lack of strong emission-line gradients in some sources may indicate that the length scale over which the photoionizing energy of an accretion source is deposited is comparable to that of a circumnuclear star-forming zone (i.e., ~100 pc), so that the influence of both energy sources is spatially commingled. This would involve a different gas distribution or geometry than is typical of the LINER 1s and Seyferts, which tend to have highly concentrated nebulosity around an accretion source, and may have interesting implications for the available fuel supply. Alternatively, a distributed ionization source, such as turbulent mixing layers (e.g., Begelman & Fabian 1990) or evolved stars (e.g., Binette et al. 1994), rather than simply a central accretion source, may be important in these nuclei; the magnetic field may also be energetically significant in these regions. A distributed source is potentially supported by our finding that transition and LINER 2 nuclei in the SUNNS sample preferentially show evidence of a nuclear component of stars with ages $\lesssim 1$ Gyr (Sarzi et al. 2005; see also González Delgado et al. 2004). Investigation of a larger sample of transition objects is important for defining the properties of these sources and determining their nature. The decrease in ionization with decreasing radius in the Seyfert 2 nuclei is likewise unexpected, and scrutiny of larger samples is needed to understand this finding. Integral-field spectroscopic observations could prove useful to understanding the role of different ionizing sources at different radii, as recently shown by Mazzuca et al. (2006) in their study of the galaxy NGC 7742, which hosts a circumnuclear starburst and an active nucleus of composite nature.

4.2. *Galaxy Nuclei: Ours and Others*

While the sample studied here consists of nearby emission nuclei, there is one such source notably missing from our study, namely the Milky Way nucleus. Integrating the Galactic center into a larger context of galaxy nuclei is complicated observationally by the large extinction to this region ($A_V \approx 31$ mag; Rieke et al. 1989) and by its close proximity, which results in an angular scale ($1'' \approx 0.1$ pc) substantially different from extragalactic sources. Spectroscopic measurements obtained for both external galaxies and the Galactic center on the *same* metric scale in the *same* bandpass remain very limited. The SUNNS data, however, offer a new basis for comparison by at least matching the approximate metric scale of many measurements of the Galactic center.

The Milky Way, like the SUNNS galaxies, is host to a low-luminosity emission nucleus. The rate of photoionizations by Lyman continuum photons for the Galactic center is tabulated as a function of radius by Mezger et al. (1996; $N'_{\rm Lyc}$ in their Table 6), based on radio measurements of free-free emission. After rescaling to a distance to the Galactic center of $R_0 = 8$ kpc, the results indicate $N'_{\rm Lyc} = 2.1 \times 10^{50}$ s^{-1} within $R = 0.9$ pc and $N'_{\rm Lyc} = 5.7 \times 10^{51}$ s^{-1} within $R = 235$ pc. The Hα luminosity L(Hα) emerging within $R = 235$ pc predicted from recombination theory with negligible extinction would be $\sim 8 \times 10^{39}$ ergs s^{-1}. Objects with this L(Hα) are common in the full Palomar spectroscopic survey, which has a slightly lower median $L(\mathrm{H}\alpha) = 2 \times 10^{39}$ ergs s^{-1} for an equivalent radius of ~140 pc (i.e., for a circular aperture with area equal to the rectangular Palomar aperture; Ho et al. 1997b). Allowing for modest extinction of the Galactic center emission and the somewhat different metric apertures would bring the Milky Way value closer to the Palomar median. For comparison purposes with SUNNS, an estimate of $N'_{\rm Lyc}$ within $R \approx 10$ pc for the Galaxy would be desirable, but is not readily available; with the existing data we can nonetheless estimate that the ratio of recombination luminosities within $R \sim 10$ and ~100 pc is approximately 1 order of magnitude, which is broadly consistent with our measured ratio for other galaxies (Fig. 2). The Galactic center is thus a very typical nucleus in terms of its nebular luminosity and concentration.

The SUNNS data provide a further basis for comparing interstellar conditions in the Galactic center with those in other galaxy

nuclei. Nebular densities within $\sim$10 pc tend to be rather high. As discussed in § 3.2, the [S II] diagnostic indicates a typical density of $\sim 10^3$ cm^{-3}, but other lines point to the presence of gas with densities of $\sim 10^4$ cm^{-3} in the SUNNS nuclei. Very similar results are found in the Galactic center, using constraints from infrared fine-structure line ratios and emission measures (e.g., Genzel et al. 1994; Beckert et al. 1996 and references therein). The *HST* spectra do not provide quantitative constraints on the gas-phase abundances, although our analysis of the *stellar* abundances with these data indicates that typical metallicities $Z \approx (1\text{–}2) \times Z_\odot$ (Sarzi et al. 2005). This range matches estimates of the nebular metallicity of the Galactic center (Shields & Ferland 1994), and estimates of metallicity for stars in the central parsecs also suggest a typical value of $Z \approx Z_\odot$ (Ramírez et al. 2000; Blum et al. 2003).

Although we cannot see the optical spectrum of the Galactic center, we can make some inferences about its optical spectral class from the results noted above and other measurements. The Galactic center provides compelling evidence for the presence of a black hole with a mass $M_\bullet \approx (3\text{–}4) \times 10^6\ M_\odot$ (e.g., Schödel et al. 2003; Ghez 2004); this mass and the stellar velocity dispersion σ_* for the Milky Way bulge are in reasonable accord with the $M_\bullet$-σ_* correlation defined by other galaxies. The central black hole is apparently accreting, based on its appearance as the compact radio source Sgr A* (Balick & Brown 1974) and an associated X-ray source (Baganoff et al. 2003). The accretion luminosity is, however, very feeble ($\lesssim 10^{37}$ ergs s^{-1}; Narayan et al. 1998 and references therein), and thus insufficient to power a significant fraction of the nebular emission. The nebular emission on scales from $\sim$1 pc (e.g., Lutz et al. 1996) to $\sim$60 pc (e.g., Simpson et al. 1999) is characterized by low-ionization lines. The lack of both a strong compact X-ray source and high-ionization nebulosity implies that the Milky Way is not a Seyfert nucleus. Likewise, the central parsec of the Galaxy does not exhibit strong, quasar-like permitted lines from high-velocity gas; the Galactic center is not a broad-line (type 1) nucleus.

Would our counterparts in other galaxies regard the Milky Way as any sort of AGN, of the types found in the Palomar spectroscopic survey? If so, our Galaxy would have to be a LINER or H II/LINER transition object. A LINER generated via photoionization is excluded, based on the absence of a significant compact hard X-ray source to power the nebulosity, as well as from detailed aspects of the infrared and radio emission lines (Shields & Ferland 1994; Lutz et al. 1996). Recent observations with *Chandra* reveal diffuse hard X-ray emission from the central $R \approx 60$ pc, with a luminosity of $\sim 2 \times 10^{36}$ ergs s^{-1} (Muno et al. 2004). While insufficient to power significant nebular emission directly, the hard X-rays are of uncertain origin, and would require a kinetic energy input of $\sim 10^{40}$ ergs s^{-1} if generated in (unbound) thermal plasma (see Muno et al. 2004 for details). If a fraction of this mechanical energy were transferred to the nebular plasma, it could modify the excitation of the gas, resulting in enhancement of optical collisionally excited lines. However, the nebular gas is clearly not heavily shocked; the plasma is not highly ionized, and at least within $\sim$6 pc of the center, the electron temperature as revealed by radio line-to-continuum ratios is only 7000 ± 500 K (Roberts & Goss 1993). While this value may be slightly higher than expected from simple stellar photoionization (Shields & Ferland 1994), it appears that the gas is not heated sufficiently to power optical forbidden lines at the level seen in LINERs.

We conclude that the center of the Milky Way would appear spectroscopically as an H II nucleus or possibly a transition object for an extragalactic optical observer. As in most of the SUNNS galaxies (Sarzi et al. 2005), the inner stellar bulge of our Galaxy is predominantly old (Blum et al. 2003; van Loon et al. 2003; although cf. Figer et al. 2004), but some star formation has occurred in recent episodes, and in the case of the Milky Way, the ultraviolet radiation from normal massive stars apparently dominates the nebular ionization. For galaxies like our own, with a Hubble type of approximately Sbc, the Palomar spectroscopic survey found that the fractions hosting H II and transition nuclei are $\sim$50% and $\sim$20%, respectively (Ho et al. 1997b). In its nebular excitation, star formation history, and relation to the larger Galaxy, the Milky Way again has a very typical nucleus.

5. SUMMARY AND CONCLUSIONS

Ground-based spectroscopic surveys indicate that the majority of galaxies host emission-line nuclei, and the SUNNS results provide new insights into the structure and energetics of these nebular sources. The findings presented here indicate that the emitting gas is spatially distributed on scales of $\sim$100 pc, with accretion-powered objects showing a significant degree of concentration in the observed emission. Within these regions, modest radial gradients in optical emission-line ratios are seen; density gradients evidently play an important role in driving these trends, although there is some evidence as well for ionization gradients in the plasma. LINER/H II transition nuclei show only mixed indications of a simple composite spatial structure, contrary to expectations, suggesting that distributed sources of ionization beyond normal O-type stars may be involved in powering these common objects.

These findings provide a framework for gauging the extent to which the center of the Milky Way is a typical galaxy nucleus. The Galactic center is very similar to other emission-line nuclei in terms of its nebular luminosity, surface brightness distribution, and ionization. Combining the present results with other published findings, it is additionally clear that the Galactic center resembles the nuclei of other systems in terms of its metallicity and stellar population, and likewise its black hole mass and probable spectroscopic class, considered in relation to the bulge properties of the host galaxy. As a laboratory for the study of galaxy nuclei, the center of the Milky Way thus provides a very representative example.

We thank the referee for constructive comments. Support for this research was provided by NASA through grant GO-7361 from the Space Telescope Science Institute, which is operated by the Association of Universities for Research in Astronomy, Inc., under NASA contract NAS5-26555.

REFERENCES

Baganoff, F. K., et al. 2003, ApJ, 591, 891
Balick, B., & Brown, R. L. 1974, ApJ, 194, 265
Barth, A. J., Ho, L. C., Filippenko, A. V., Rix, H.-W., & Sargent, W. L. W. 2001, ApJ, 546, 205
Beckert, T., Duschl, W. J., Mezger, P. G., & Zylka, R. 1996, A&A, 307, 450
Begelman, M. C., & Fabian, A. C. 1990, MNRAS, 224, 26
Binette, L., Magris, C. G., Stasinska, G., & Bruzual, A. G. 1994, A&A, 292, 13
Blum, R. D., Ramírez, S. V., Sellgren, K., & Olsen, K. 2003, ApJ, 597, 323
Bohlin, R., & Hartig, G. 1998, STIS Instrument Science Report 98-20 (Baltimore: STScI)
Bower, G. A., Wilson, S., Heckman, T. M., & Richstone, D. O. 1996, AJ, 111, 1901
Bruzal, G., & Charlot, S. 2003, MNRAS, 344, 1000
Cid Fernandes, R., et al. 2004, ApJ, 605, 105
de Vaucouleurs, G., de Vaucouleurs, A., Corwin, H. G., Jr., Buta, R. J., Paturel, G., & Fouqué, R. 1991, Third Reference Catalog of Bright Galaxies (New York: Springer)

Eracleous, M., & Halpern, J. P. 2001, ApJ, 554, 240
Ferrarese, L., & Merritt, D. 2000, ApJ, 539, L9
Figer, D. F., Rich, R. M., Kim, S. S., Morris, M., & Serabyn, E. 2004, ApJ, 601, 319
Filippenko, A. V., & Halpern, J. P. 1984, ApJ, 285, 458
Filippenko, A. V., & Sargent, W. L. W. 1985, ApJS, 57, 503
Filippenko, A. V., & Terlevich, R. 1992, ApJ, 397, L79
Gebhardt, K., et al. 2000, ApJ, 539, L13
Genzel, R., Hollenbach, D., & Townes 1994, Rep. Prog. Phys., 57, 417
Ghez, A. M. 2004, in Coevolution of Black Holes and Galaxies, ed. L. C. Ho (Cambridge: Cambridge Univ. Press), 53
González Delgado, R. M., Cid Fernandes, R., Pérez, E., Martins, L. P., Storchi-Bergmann, T., Schmitt, H., Heckman, T., & Leitherer, C. 2004, ApJ, 605, 127
Hao, L., et al. 2005, AJ, 129, 1783
Häring, N., & Rix, H.-W. 2004, ApJ, 604, L89
Ho, L. C., Filippenko, A. V., & Sargent, W. L. W. 1997a, ApJS, 112, 315
———. 1997b, ApJ, 487, 568
Ho, L. C., Filippenko, A. V., Sargent, W. L. W., & Peng, C. Y. 1997c, ApJS, 112, 391
Ho, L. C., Rudnick, G., Rix, H.-W., Shields, J. C., McIntosh, D. H., Filippenko, A. V., Sargent, W. L. W., & Eracleous, M. 2000, ApJ, 541, 120
Ho, L. C., Sarzi, M., Rix, H.-W., Shields, J. C., Rudnick, G., Filippenko, A. V., & Barth, A. J. 2002, PASP, 114, 137
Hughes, M. A., et al. 2003, AJ, 126, 742
Kaufman, V., & Sugar, J. 1986, J. Phys. Chem. Ref. Data, 15, 321
Kennicutt, R. C., Keel, W. C., & Blaha, C. A. 1989, AJ, 97, 1022
Kewley, L. J., Dopita, M. A., Sutherland, R. S., Heisler, C. A., & Trevena, J. 2001, ApJ, 556, 121
Kormendy, J., & Richstone, D. O. 1995, ARA&A, 33, 581
Kriss, G. 1994, in ASP Conf. Ser. 61, Astronomical Data Analysis Software and Systems III, ed. D. R. Crabtree, R. J. Hanisch, & J. Barnes (San Francisco: ASP), 437
Lutz, D., et al. 1996, A&A, 315, L269
Mazzuca, L. M., Sarzi, M., Knapen, J. H., Veilleux, S., & Swaters, R. 2006, MNRAS, in press (astro-ph/0607518)
Mezger, P. G., Duschl, W. J., & Zylka, R. 1996, A&A Rev., 7, 789
Muno, M. P., et al. 2004, ApJ, 613, 326
Narayan, R., Mahadevan, R., Grindlay, J. E., Popham, R. G., & Gammie, C. 1998, ApJ, 492, 554
Osterbrock, D. E. 1989, Astrophysics of Gaseous Nebulae and Active Galactic Nuclei (Mill Valley: Univ. Science Books)
Pelat, D., Alloin, D., & Fosbury, R. A. E. 1981, MNRAS, 195, 787
Peterson, B. M. 1997, An Introduction to Active Galactic Nuclei (Cambridge: Cambridge Univ. Press), 94
Ramírez, S. V., Sellgren, K., Carr, J. S., Balachandran, S. C., Blum, R., Terndrup, D. M., & Steed, A. 2000, ApJ, 537, 205
Rieke, G. H, Rieke, M. J., & Paul, A. E. 1989, ApJ, 336, 752
Rix, H.-W., & White, S. D. M. 1992, MNRAS, 254, 389
Roberts, D. A., & Goss, W. M. 1993, ApJS, 86, 133
Rudnick, G., Rix, H.-W., & Kennicutt, R. C., Jr. 2000, ApJ, 538, 569
Sanchez-Blazquez, P., et al. 2006, MNRAS, in press (astro-ph/0607009)
Sarzi, M., Rix, H.-W., Shields, J. C., Ho, L. C., Barth, A. J., Rudnick, G., Filippenko, A. V., & Sargent, W. L. W. 2005, ApJ, 628, 169
Sarzi, M., Rix, H.-W., Shields, J. C., Rudnick, G., Ho, L. C., McIntosh, D. H., Filippenko, A. V., & Sargent, W. L. W. 2001, ApJ, 550, 65
Sarzi, M., et al. 2002, ApJ, 567, 237
———. 2006, MNRAS, 366, 1151
Schödel, R., Ott, T., Genzel, R., Eckart, A., Mouawad, N., & Alexander, T. 2003, ApJ, 596, 1015
Shields, J. C., & Ferland, G. J. 1994, ApJ, 430, 236
Shields, J. C., Rix, H.-W., McIntosh, D. H., Ho, L. C., Rudnick, G., Filippenko, A. V., Sargent, W. L. W., & Sarzi, M. 2000, ApJ, 534, L27
Simpson, J. P., Witteborn, F. C., Cohen, M., & Price, S. D. 1999, in ASP Conf. Ser. 186, The Central Parsecs of the Galaxy, ed. H. Falcke et al. (San Francisco: ASP), 527
Storchi-Bergmann, T. 1991, MNRAS, 249, 404
Tully, R. B. 1988, Nearby Galaxies Catalog (Cambridge: Cambridge Univ. Press)
van Loon, J. T., et al. 2003, MNRAS, 338, 857
Veilleux, S., & Osterbrock, D. E. 1987, ApJS, 63, 295
Véron, P., Gonçalves, A. C., & Véron-Cetty, M.-P. 1997, A&A, 319, 52
Wiese, W. L., Smith, M. W., & Glennon, B. M. 1966, Atomic Transition Probabilities: A Critical Data Compilation (Washington, DC: National Bureau of Standards)